Are there similarities between quasi-static indentation and low velocity impact tests for flax-fibre composites?

Adélaïde Leroy, Daniel Scida, Émile Roux, Franck Toussaint, Rezak Ayad

Are there similarities between quasi-static indentation and low velocity impact tests for flax-fibre composites?

Adélaïde Leroy[1], Daniel Scida[1], Emile Roux[2], Franck Toussaint[2], Rezak Ayad[1]

[1] Université de Reims Champagne Ardenne, ITheMM (EA 7548), F-51097, Reims, France
[2] Université Savoie Mont Blanc, SYMME, F-74000 Annecy, France

---

Abstract

Flax-fibre composites are increasingly used as a replacement of classical synthetic composite materials. Due to the good energy absorption properties of flax fibres, they represent a promising alternative in structures susceptible to low velocity impact (LVI) damage. However, this type of dynamic loading is complex, expensive to perform and not necessarily easy to fully investigate. A simpler way to tackle this problem consists in investigating quasi-static indentation (QSI) tests, but this alternative remains relatively under-researched for natural fibre composites. Thus, this paper aims at providing a comparison between both types of loading to facilitate the later analysis and modelling of flax fabric laminates submitted to LVI. Six layers of a flax 2/2 twill fabric were used as reinforcement for epoxy laminates made through vacuum infusion. Specimens were then submitted to instrumented LVI and QSI tests at comparable energy levels, with a 1.5% to 3.9% difference only. Load-displacement curves and visible damage were first analysed and compared between both test types. Then, the internal damage within QSI specimens were investigated using acoustic emission (AE). Our findings showed good analogies between both testing methods in all the stages of damage development. Great similarities were found in load-displacement curves (in shape, stiffness and peak load), in energy absorption capacity (at 5 and 10 J) and in

* Corresponding author. Tel.: +33 325 427 144
E-mail address: adelaide.leroy@univ-reims.fr

visible damage. Actually, the differences between QSI and LVI remain low, i.e. 2.1% for linear stiffness, from 0.2 to 5.6% for peak load and less than 7% for the proportions of absorbed energy. Comparison of the QSI damage analysed from the AE data with LVI results from literature suggested similar mechanisms and onset sequences. These results revealed that QSI monitoring could provide characteristic indications on the damage evolution of flax-fibre woven composites during an LVI test.

Keywords: flax-fibre composites; low velocity impact; quasi-static indentation; experimental investigation; acoustic emission; analogy

1. Introduction

Plant fibres have been increasingly used as composite reinforcement in the last decades. Despite their inherent variability that may impact the final properties of composites (Baley et al., 2020; Haag et al., 2017; Le Gall et al., 2018), they exhibit many advantages over their synthetic counterparts, such as lower environmental impact, good acoustic insulation and vibration damping, high specific mechanical properties, low cost and safe handling (Amiri et al., 2017; Correa et al., 2019; Dicker et al., 2014). Flax-fibre composites, in particular, are commonly used for non-structural or semi-structural applications. Recently, several research works have addressed the development of high performance biocomposites for structural applications (Baley et al., 2020; Le Duigou et al., 2019; Zuccarello et al., 2018). In this respect, the properties of flax fibres make them suitable for use as reinforcement of composites subjected to low velocity impact (LVI). One common test method used to assess the LVI performance of plant-fibre composites is drop-weight impact, which is very similar to a real impact scenario (Agrawal et al., 2014; Sutherland, 2018).

Despite these advantages, literature specifically addressing the impact resistance of composite laminates with long continuous natural fibres submitted to a drop weight impact is not extensive (Muneer Ahmed et al., 2021). Some studies have been conducted on woven composites based on jute fibres (Dhakal et al., 2014) or hemp fibres (Scarponi et al., 2016), and on unidirectional, cross-ply and woven flax fabric composites (Awais et al., 2020; Bar et al., 2020; Bensadoun et al., 2017; Liang et al., 2015; Ravandi et al., 2017; Sy et al., 2018). The type of fibre architecture can have an effect on the impact resistance. Bar et al. (Bar et al., 2020) found that flax plain woven composites were better than UD composites, mainly due to interlaced structure of plain woven fabric. Sy et al. (Sy et al., 2018) reported that cross-ply flax/epoxy laminates exhibited higher penetration threshold energy and impact toughness compared to their unidirectional counterparts. The damage progression during LVI may also evolve. Liang et al. (Liang et al., 2015) investigated the fracture mechanism of quasi-isotropic flax/epoxy composites and found that delaminations occurred first, at low energy levels, followed by the development of intra-laminar transverse cracks resulting from fibre failure. From an X-ray micro-computed tomography study, Miqoi et al. (Miqoi et al., 2021) suggested a damage scenario for the impacted woven composite. They stated that matrix cracking first appeared on the un-impacted surface and propagated along the yarns in a transverse and longitudinal path. When the energy was sufficiently high, it developed into delamination which propagated between the damaged yarn and the perpendicular yarn just below.

Another type of loading that creates damage in laminates and resembles LVI is Quasi-Static Indentation (QSI). A QSI test consists in applying on the material a transverse load perpendicular to the indented surface via a hemispherical indenter.

Whereas the impactor of an LVI drop tower test is in free fall before hitting the surface of the composite, the indenter of a QSI test is brought into contact with the surface prior to the test. Thus, both testing methods are comparable in their working principle, except that one is dynamic in nature (LVI) while the other is quasi-static (QSI). However, an LVI corresponds to an impact event in which the contact time of the impactor on the material surface is long compared to the propagation time of the stress-wave induced by the impact, making it close to static loading (Andrew et al., 2019). Consequently, several authors have compared LVI with QSI, particularly for carbon-fibre/epoxy laminates, sometimes recommending the use of indentation to analyse and better understand impact damage mechanisms (Nettles and Douglas, 2002; Saeedifar et al., 2018; Serna Moreno and Horta Muñoz, 2020; Spronk et al., 2018; Wu et al., 2020).

As a matter of fact, the implementation and instrumentation of LVI drop tower tests is often challenging. These tests require the use of special equipment (drop tower). They usually have a short duration, making it hard to investigate the damage sequence. The roughness of an impact limits the use of recording devices such as acoustic emission sensors. Moreover, load-displacement curves may be hard to read and interpret due to the presence of oscillations that result from the dynamic nature of the test. Conversely, QSI tests can be carried out on a universal testing machine, requiring as additional equipment only an indenter and a specific equipment for fixing the specimen. Additionally, QSI maximum displacement can easily be monitored to investigate the damage sequence. Finally, the acoustic emission technique can be implemented safely, low acquisition rates suffice, and load-displacement curves are exempt of oscillations.

Nevertheless, the question arises regarding the potential use of QSI test in complement to LVI test. Some authors did not find any significant differences between both tests whereas others reported non-negligible dissimilarities. The study conducted by Nettles and Douglas (Nettles and Douglas, 2002) on quasi-isotropic carbon/epoxy laminated plates showed no distinct differences between QSI and LVI tests based on the maximum applied transverse load. Likewise, Suresh Kumar et al. (Suresh Kumar et al., 2017) reached the same conclusion on quasi-isotropic glass/epoxy, glass/basalt/epoxy and glass/carbon/epoxy composite laminates. Their results indicated that there were no significant differences with regard to the dent depth, back surface crack size and load-deflection behaviour. In particular, the changes in peak contact force and residual deformation were similar. Saeedifar et al. (Saeedifar et al., 2018) also found that the general behaviour of two quasi-isotropic carbon/epoxy laminates under QSI and LVI tests showed great similarity. However, they reported two differences: about 10% maximum difference of the delaminated area and a significant increase in the critical load corresponding to the initial delamination growth for the LVI tests compared to the indentation tests. In (Wu et al., 2020), the QSI results for two carbon fibre braided composites were in good agreement with LVI tests before the peak load. After the peak load, the load measured in QSI was slightly higher than the impact load in LVI test. As a result, it was concluded that QSI tests for braided laminates could be used to analyse the damage onset and development during an impact event. In a paper of Zhang et al. (Zhang et al., 2015), the LVI and QSI tests on carbon/bismaleimide laminates resulted in a similar delamination shape and a similar general trend of delamination size throughout the thickness direction. In conclusion of their study, the authors claimed that using QSI-induced damage to replace LVI-induced damage made it possible to assess approximately equivalent strength in static compression, which was not recommended for compressive fatigue strength. The finding is completely different in another study on carbon/epoxy and glass/polyamide-6 composites based on cross-ply or quasi-isotropic stacking sequences (Spronk et al., 2018). Differences between both tests were found on the load-displacement response and were significant for the glass/polyamide-6 composite due to the constituent rate-dependency. Although some characteristics were relatively similar, the conclusion came down to the fact that the LVI and QSI test methods cannot be exchanged for material characterisation, according to the authors. Some differences in the first slope of the load-displacement curve were also found on $[\pm 45]_{4s}$ carbon fibre laminates since the laminate under LVI was 36% stiffer than in the QSI test (Serna Moreno and Horta Muñoz, 2020). However, similar levels of internal energy were found in the most notable events during the loading process. The results of Goodarz et al. (Goodarz et al., 2019) suggested that the limit of applicability of the quasi-static analysis for the dynamic problem of aramid/epoxy plain-weave laminates (with nanocomposites interlayers) was at impact energy level before beginning plate penetration. Zulkafli et al. (Zulkafli et al., 2020) investigated the effects of stacking sequence of hybrid cross-ply banana/glass fibre reinforced polypropylene composites on QSI and LVI. By comparing the damage assessment of the QSI and LVI specimens, the difference observed was located at the fracture level, since the LVI specimen was more brittle than the QSI specimen. According to the authors, this can be explained by the sudden impact applied to the specimens. It should also be noted that the damage area of the LVI specimens was much larger than the QSI specimens.

In summary, some of the available conclusions on a QSI/LVI comparison are contradictory and there is no real consensus on whether both tests are equivalent. Moreover, to the best of the authors' knowledge, such a comparison for non-hybrid natural-fibre laminates has never been the main subject of investigation in any study. Up until now, such comparisons have been conducted for the sole purpose of providing a reference in the very few studies that deal with hybrid laminates (Jusoh et al., 2017; Malingam et al., 2018). This lack of consensus and data has prompted us to carry out our own investigations on the similarities between LVI and QSI for woven flax/epoxy laminates, with a double aim: (*i*) providing indications and advice to researchers and industrials who would be thinking of replacing LVI with the cheaper and more convenient QSI testing method; (*ii*) laying the foundation of our future work, which will consist in gaining a deeper insight into impact damage mechanisms and in proposing analytical and numerical models of LVI. For this purpose, flax twill-weave fabric laminates were manufactured using vacuum infusion process and then subjected to impact and indentation tests. Next, the obtained load-displacement curves were analysed separately and concomitantly for different levels of energy. The LVI/QSI comparison was also conducted on the absorbed energies in relation to the total energy. Finally, post-impact images and data obtained from a detailed analysis of the AE signals were used to study the damage occurring within the impacted and indented laminates.

2. Material and methods

2.1 Material and manufacturing process

A 2/2 twill fabric of flax untwisted rovings, with a surface weight of 360 g/m², was supplied by Depestele Group and used as reinforcement for our composites. Rectangular-shaped samples were cut out of the fabric roll to the dimensions of 350 x 400 mm² and stacked on top of each other to form a 6-layer preform. All plies were oriented in the same direction. The preform was then impregnated with the matrix via vacuum infusion as depicted in Fig. 1. The matrix consisted of epoxy resin SR 8100 and hardener SD 8823, both provided by Sicomin and mixed according to the ratio of 100/26 by weight. In order to infuse the preform with the matrix, a vacuum was applied under a 0.6 bar pressure at room temperature. After a polymerization phase at room temperature for 24 hours, the composite plate was cured in an oven at 40 °C for 24 more hours, as recommended by the supplier. The resulting plate had a fibre volume fraction of 31.26 ± 0.57%. An average void content of 1.43 ± 0.72% was obtained on the samples extracted from the plate. The fibre volume fraction v_f of the studied composite was experimentally determined by weighing the cured plate M_c, the dry fabrics M_f and by taking into account the mass density of fibres (ρ_f = 1450 kg·m^{-3}) and matrix (ρ_m = 1100 kg·m^{-3}), from the following equation:

$$v_f = \frac{1}{1+\left(\frac{M_c-M_f}{M_f}\right)\left(\frac{\rho_f}{\rho_m}\right)} \tag{1}$$

The void content v_v was experimentally determined from the mass M_c and dimensions l, w and h (length, width and thickness) of the composite samples, the number of layers n, the area density of the dry fabric ρ^s_f and the fibre and matrix mass densities ρ_f and ρ_m, by using the following equation (Scida et al., 2013)

$$v_v = 1 - \frac{M_c}{l \cdot w \cdot h \cdot \rho_m} + \frac{n \cdot \rho_f^s}{h} \cdot \left(\frac{1}{\rho_m} - \frac{1}{\rho_f}\right) \tag{2}$$

Finally, 100 x 150 mm^2 specimens with a thickness of 4.77 ± 0.123 mm were obtained from the plates by laser cutting.

Insert Fig. 1 here

2.2 Low-Velocity Impact (LVI) test

LVI tests were performed on a drop tower with a hemispherical impactor at energies of 5, 10, 15 and 20 J, as depicted in Fig. 2a. The tower was built by the SYMME laboratory during the PhD thesis of Cuynet (Cuynet, 2018). The drop height was up to 2 m, allowing to reach a maximum velocity of 6.3 m/s. The impactor, with a diameter of 14.7 mm, was rigidly screwed to a platform that could slide up and down almost freely along a rail. Different weights could be added on the platform. The falling mass, which was fixed at 2948 g, was then dropped from different heights to obtain the desired impact energy (5, 10, 15 or 20 J) according to the equation $E_{imp} = mgh$, where E_{imp} is the impact energy in J, m the mass dropped in kg, g the standard gravity in m.s^{-2} and h the height in m. A system used to keep the specimen in place was fixed at the bottom of the tower. It consisted of a die and a holder, both with a circular opening 80 mm in diameter. The tower was instrumented with a load sensor (maximum sampling frequency of 100 kHz) and an accelerometer (acceleration range of 50 g) placed above the impactor and used in order to record load and acceleration values respectively. The speed and displacement of the impactor were calculated via the double integration of acceleration, as explained in (Cuynet et al., 2018).

Insert Fig. 2 here

2.3 Quasi-Static Indentation (QSI) test

QSI tests were performed on an Instron universal testing machine model 3382 used to apply the loading. A special experimental device initially designed at the SYMME laboratory to characterize the mechanical behaviour of titanium specimens (Pottier et al., 2012) was mounted on the Instron testing machine (Fig. 2b). It was composed of a rigid stainless-steel frame fixed to the machine base in place of the lower holding grip. A hemispherical indenter similar to the LVI impactor was rigidly screwed to the moving crosshead in place of the upper grip. Note that in the rest of the paper the term "indenter" is used to refer to the QSI test and "impactor" to the LVI test. The system used on top of the indentation unit to keep the specimen in place was the same as the one used for LVI. Prior to testing, the indenter was put on the surface of the tested specimen with a preload lower than 10 N. Each specimen was submitted to one loading cycle. The aim was to simulate an impact with a rebound. Tests were carried out at a loading rate of 1.5 mm/min. For each energy level, the mean value of all recorded LVI maximum deflections was determined and used to set the maximum displacement of the indenter: 4.15 mm for 5 J, 6.04 mm for 10 J, 9.55 mm for 15 J and 12.06 mm for 20 J. The average energies obtained from such monitoring were similar to LVI (1.5% to 3.9% higher). The applied load and the displacement of the indenter were recorded by the inbuilt sensors of the testing machine. To check the accuracy of measurements, an LVDT sensor was set up during the first tests. Measurements from the machine exhibited a lower than 1% difference in displacement with the LVDT. Therefore, the data obtained via the testing machine was considered sufficiently accurate and reliable, and the LVDT sensor was subsequently removed.

2.4 Acoustic Emission (AE)

AE was continuously monitored during indentation tests to obtain information about damage evolution. AE events were recorded with a PCI-2 AE system developed by Mistras Group Company. The two-channel data acquisition system had a sampling rate of 5 MHz and a pre-amplification of 40 dB. AE signals were detected through two resonant Micro-80 piezoelectric sensors with a frequency range of 100 kHz–1 MHz and a resonance peak around 300 kHz. The threshold level was set up as 32 dB and the system timing parameters were: peak definition time PDT = 30 μs, hit definition time

HDT = 200 μs and hit lockout time HLT = 300 μs. PDT, HDT and HLT enabled the selection of the event characteristics. The sensors were kept in place on the upper surface of the specimens by two metallic arms with springs and rubber pads screwed to the specimen fixture system, as depicted in Fig. 2b. A silicon grease was used to ensure good acoustic coupling. Before testing, the data acquisition system was calibrated according to pencil lead breaks.

3. Results and discussion

3.1 Load-displacement data

3.1.1 Concepts and terminology

Data obtained from LVI and QSI tests is commonly represented as load-displacement curves in which the load applied to a specimen by the impactor or indenter is plotted against its vertical displacement. A typical QSI curve is shown in Fig. 3a. All the remarks and definitions regarding this figure also apply to the results of LVI tests. The curve is divided into two parts according to the evolution of the displacement values. Whereas they increase in the first part due to the indenting of the specimen, the rise of the impactor during rebound (LVI) or the rise of the indenter during unloading (QSI) results in a decrease of displacement values in the second part. On the one hand, the first part of the curve can be further divided into Stage 1, relatively linear, and Stage 2, with a saw tooth pattern due to a multitude of discontinuities in load, as can be seen in Fig. 3b. On the other hand, Stage 3 corresponds to rebound or unloading. Here, the curve does not return towards the origin of the graph because for greater clarity load is plotted as a function of time instead of displacement.

Insert Fig. 3 here

Some important concepts used in this paper are defined below and illustrated in Fig. 3a:

- First Load Drop (FLD) corresponds to the first drop in load on the load-displacement curve and marks the boundary between Stages 1 and 2.
- Peak Load (L_p) is the maximum value of load recorded during an LVI or QSI test.
- Load at Maximum Displacement (L_{dmax}) is the load value of the point corresponding to the maximum displacement. This point marks the end of Stage 2 and the beginning of Stage 3.
- Residual Displacement (d_{res}) corresponds to the displacement value of the last point at the end of Stage 3. Its value reflects the permanent deformation of the specimen.
- Absorbed Energy (E_a) is the amount of energy absorbed by the specimen during an impact event or an indentation loading cycle. It corresponds to the area of the hysteresis loop, which is the area inside the load-displacement curve.
- Recovered Energy (E_r) is the amount of energy that is not absorbed but returned to the impactor during rebound (LVI) or to the indenter during unloading (QSI). It is equal to the area below Stage 3 of the curve.
- Total Energy (E_t), also called Impact or Indentation Energy, is the amount of energy involved in an LVI or QSI test (not represented in Fig. 3a). It corresponds to the sum of absorbed and recovered energies. When $E_t = E_r$, the specimen reacts elastically to the force. When $E_t = E_a$, the impactor or indenter perforates the specimen through its full thickness.

Note that the method used to calculate the areas under the curve was the trapezoidal rule from trapezoids built with the measurement points.

3.1.2 LVI / QSI comparison

In this study, LVI and QSI tests were performed at four different levels of total energy: 5, 10, 15 and 20 J. The superimposed load-displacement curves for LVI are shown in Fig. 4a. For each energy level, the most representative curve was selected and smoothed to eliminate the original oscillations resulting from stored elastic energy, inertial effects and reflected stress waves (Feraboli, 2006). Similarly, Fig. 4b shows the superimposed most representative load-displacement curves for QSI, which do not require any smoothing. In both cases, the curves overlap well in their initial part (Stage 1 and beginning of Stage 2), showing the good repeatability of LVI and QSI tests. The curves exhibit similar shapes, except for a total energy of 20 J, where Stage 3 is significantly different due to the initiation of specimen perforation.

Insert Fig. 4 here

As the level of total energy increases, Stage 2 occupies a more substantial portion of the loading phase, the permanent deformation of specimens being more important. This observation is corroborated by a rise in residual displacement and suggests many damage initiation and/or propagation events within the material. In contrast, Stage 1 remains similar at all energy levels. The absence of abrupt changes in load values and the relative linearity suggest a little or no damage. The main characteristics of this stage are summarized in Table 1 from their average and standard deviation values. The linear stiffness corresponds to the average slope of the curve until the FLD occurs (Nisini et al., 2017) and is very similar for LVI and QSI, with a difference of only 2.1%.

However, QSI load and displacement values at FLD are 13% lower than LVI. This does not necessarily imply a substantial difference in the onset of damage. Indeed, oscillations have been removed by smoothing the LVI curves, providing only an estimation of load and displacement values at FLD, especially as the number of data points is very limited in this area. Thus, FLD may actually occur between two spaced data points before the first visible impact load drop, accounting for higher LVI values.

Insert Table 1 here

This lack of data, due to high impactor speed and limited sampling frequency of the load sensor, is clearly visible in Fig. 5. In each graphic plotting, corresponding to a certain energy level, a representative QSI curve is superimposed to a representative LVI curve. Despite the limited amount of data in Stage 1, we observe an initial irregularity related to inertial loading. This phenomenon is caused by the rigid-body acceleration of the specimen from its original rest position to the velocity of the impactor (Feraboli, 2006). In QSI curves, the small irregularity is characteristic of flexural loading.

Insert Fig. 5 here

Even after these initial irregularities, the linearity of Stage 1 is not perfect, suggesting minor damage before Stage 2 in both types of tests. This point will be further discussed in section 3.2 on damage study. At all energy levels, LVI and QSI curves exhibit similar shapes and overlap well, indicating similarities in damage mechanisms and sequence between impact and indentation. In Stage 2, load keeps increasing non-linearly until it reaches a peak. Average peak loads L_p are similar between LVI and QSI with a 0.2 to 5.6% difference, and both increase with the energy level (Fig. 6). The values of load at maximum displacement L_{dmax} are usually lower than L_p values and this difference increases from less than 1% at 5 and 10 J to 2.5% at 15 J and 37% at 20 J. This suggests that major damage mechanisms occur within the material beyond L_p at 15 and 20 J, leading to a reduction of impact or indentation resistance due to penetration and then perforation at a sufficiently high energy level.

Insert Fig. 6 here

3.1.3 Energy absorption capacity

As explained in paragraph 3.1.1, absorbed energy E_a, recovered energy E_r and total energy E_t can also be determined from load-displacement curves. E_a can then be plotted as a function of E_t, as shown in Fig. 7. Each dot in the graph represents the mean of all E_a values for a certain energy level. A set of dots linked together refers to one type of test, LVI (dashed line) or QSI (continuous line). The bars associated with each dot represents the standard deviation to the mean. The diagonal line represented above the two sets of dots is where $\underline{E_a}$ equals E_t, corresponding to the case where E_t is entirely absorbed by the specimen (complete perforation). All values within the hatched area are impossible, as E_a cannot be higher than E_t.

Insert Fig. 7 here

The graph shows great similarities between LVI and QSI, especially at 5 and 10 J, suggesting comparable behaviour between both types of loading. As can be seen in Table 2, the proportion of absorbed energy relative to total energy increases with the energy level, implying more damage. Each set is relatively linear and parallel to the diagonal, reflecting the increasing the E_a / E_t ratio. The two circled dots on the right correspond to perforation initiation, hence the higher proportion of E_a. It is assumed that at higher energy levels, data points would further approach the diagonal and ultimately reach it. As the E_a / E_t ratio approaches 1 at 20 J (0.96 for LVI and 0.91 for QSI), the energy of complete perforation is higher than 20 J. For LVI, an experimental value of 22 ± 1.3 J was found by Cuynet (Cuynet, 2018). This value for LVI suggests that complete perforation would occur at a slightly higher energy level for QSI due to the slightly lower ratio E_a / E_t at 20 J. At the other end of the sets, below 5 J, E_a should theoretically reach 0 during Stage 1, corresponding to the end of elasticity. The calculated and averaged areas under LVI and QSI Stage 1 curves correspond to approximately 2.4 J and 1.8 J respectively. The end of elasticity must thereby be reached at an energy level lower than these values.

Insert Table 2 here

3.2 Damage study

3.2.1 Visible damage observation

Part of the damage generated during an impact event or an indentation loading cycle can be seen from the outside. Fig. 8 shows the evolution of visible damage in QSI specimens tested at all four energy levels. Similar pictures of 8-ply laminates submitted to different impact energies are also presented in Fig. 9 (Cuynet et al., 2018). Despite the number of plies is different, the evolution of visible damage is the same as for 6-ply specimens. For both types of tests, marks are visible on the impacted/indented and opposite faces, but their visual characteristics are different on each side.

On the impacted or indented face, the hemispherical impactor or indenter leaves a circular imprint. The higher the energy level, the larger the imprint. Cracks can also be seen in the imprint at and above an energy level corresponding to approximatively 75% of perforation initiation energy. A difference can be observed at perforation initiation energy between LVI and QSI, as the imprint resulting from an impact exhibits a more regular and clearly defined edge. This may be due to the difference in test durations, as an LVI event lasts less than 20 ms and a QSI loading cycle more than 4 min. During an impact, material beneath the impactor may thereby be pushed outwards more violently and break more abruptly at the circumference of the imprint compared to QSI.

Insert Fig. 8 and Fig. 9 here

On the opposite face, a cross-shaped mark made of two perpendicular cracks appears right below the impact/indentation point. The cracks develop along the warp and weft directions of the flax woven reinforcement. Fig. 10 shows average crack length values at different energy levels for QSI and LVI. Total energies are normalised for both test types by the maximum total energy. The evolution of crack length follows the same trend for QSI and LVI, increasing until it reaches a plateau at approximatively 75% of perforation energy. This corresponds to the first cracks observed in the imprint on the impacted/indented face. After that, value of crack length stabilises: the energy absorbed is not used to extend the cracks anymore but to open them, pushing outwards the four corners of material delimited by the cracks. Like the edge of the imprints, folds at corners base are sharper on LVI specimens, which may also be due to the short duration of an impact compared to a QSI loading cycle. Crack stabilisation also indicates that the penetration energy threshold is similar for QSI and LVI tests and corresponds to 75% of perforation initiation energy.

Insert Fig. 10 here

3.2.2 Internal damage chronology from AE analysis

In the present study, the AE technique was used to monitor damage evolution during QSI tests only. Indeed, it was difficult to implement this technique during an impact due to the dynamic nature of LVI tests and the fragility of the sensors. Four parameters of acoustic signals were used to study the damage mechanisms and evolution: amplitude, duration, absolute energy and number of counts to peak. For a more comprehensive damage characterisation, AE information was also analysed together with mechanical information via the Sentry Function (SF). This function originally proposed by Minak and Zucchelli (Minak et al., 2009; Minak and Zucchelli, 2008) is defined by:

$$f(x) = \ln\left(\frac{E_S(x)}{E_{AE}(x)}\right) \tag{3}$$

where E_S and E_{AE} are the strain energy and cumulative acoustic energy of the material in relation to the displacement x. Thus, SF makes it possible to take into account quantitatively two phenomena: the storage of strain energy when a material is submitted to loading and the release of stored energy when internal failures occur. As the acoustic energy represents an important part of the released energy, it can be used to evaluate the strain energy storing capability of the material. As damage due to internal failure increases, the cumulated acoustic energy also increases while the amount of stored mechanical strain energy decreases. SF variations are described in detail in literature (Monti et al., 2016; Saeedifar et al., 2018; Suresh Kumar et al., 2017) and can be summarised thus in four behaviours:

- The SF curve increases in the early stages of loading, when stored energy increases due to increasing strain and AE energy remains negligible since there is no noticeable damage progression.

- A sudden drop in the SF curve corresponds to an instantaneous increase of acoustic energy, indicating macroscopic and severe damage.
- A constant trend corresponds to an equilibrium state between mechanical and acoustic energy.
- A decreasing trend is generally an indication for incipient failures and in particular, if it occurs after a sudden drop, it reveals growing damage and the degradation of the material losing its load-bearing capability.

From the AE and SF data, three different AE curves were plotted against corresponding load-displacement curves and were all expressed as a function of displacement: the number of acoustic hits, the absolute energy and the SF shown in Fig. 11a, b and c respectively. Each row in Fig. 11 corresponds to an energy level, 5, 10 and 15 J from top to bottom. At 20 J, AE was not implemented for similar reasons as in the case of LVI (risk of damaging the sensors).

Insert Fig. 11 here

The cumulative hits of Fig. 11a clearly highlight the first two stages of QSI load-time curves already described in section 3.1.1. For the sake of clarity, Stage 3 was not represented to avoid the return of the load-displacement curve associated with unloading. Overall, the curve is relatively linear in each stage, with a slope that is low in Stage 1 and much higher in Stage 2. Indeed, during this stage, the number of cumulated events skyrockets, transitioning from a low value at the end of Stage 1 to nearly the maximum value at the beginning of Stage 3. This indicates that most damage occur in Stage 2, confirming deductions made from load-displacement results. While the number of AE hits remains quite low in Stage 1, it is higher than zero. First recorded hits appear very early during testing but are limited in number, suggesting micro-damage within the specimen. As the applied load increases and approaches FLD, the number of AE events rises too, especially near FLD, where the slope of AE curves deflects sharply. Thus, FLD seems to correspond to the first significant macro-damage within the material. Fig. 11b confirms this since the AE energies are the highest near FLD.

As can be seen in Fig. 11c, SF versus displacement curves follow a similar trend at 5, 10 and 15 J, which can be divided into four zones. The first one (Zone I) corresponds to the beginning of the curve in which SF varies significantly until reaching a first plateau. After this almost constant trend (Zone II), a sudden and significant drop occurs (Zone III) followed by a new plateau (Zone IV). Once these four zones were identified, they were indicated on the graphs of Fig. 11b for a more convenient analysis of the AE signals. This analysis, conducted for each zone separately, was based on previous work. A study on a similar composite, i.e. a flax fibre 2/2 twill weave composite, investigated the damage mechanisms based on a multi-parameter analysis of acoustic signals (Saidane et al., 2019). The results showed that the signals can be classified into 4 classes A, B, C and D from four main AE characteristics (Amplitude, Energy, Duration, Counts). In accordance with literature results and observations from the fracture surfaces, the signals of Classes A, B, C and D were associated to mechanisms related to matrix cracking, fibre-matrix debonding, delamination and fibre failure respectively. The values of these classification parameters were used to analyse the signals recorded during the QSI tests.

In Zone I, the first recorded signals are all class A, associated with matrix cracking. These few events, characterised by low amplitude (< 50 dB) and low energy (< 70 aJ), explain the first drops in the SF curve. Some micro matrix cracking occurs within the specimen, without degrading its overall stiffness. Note an increase of SF before the first drop for the 15J-QSI test. This trend occurs during the first stages of loading, where AE energy is negligible, and no significant damage occurs in the laminate. From approximately 0.45 mm displacement and 300-350 N load, the SF curve in Zone II shows a relatively constant trend with the occurrence of some low intensity drops. In theory, SF remains constant when the mechanical energy and the AE energy have equilibrium state. Class A damage is still highly dominant, indicating multiple cracks, but class B signals arise with a ratio of 2.5%. These first class B signals indicate the beginning of fibre-matrix debonding, which does not yet degrade the stiffness of the specimen. The occurrence of some signals that are much more energetic and belong to the C class explain some low intensity drops in the SF curve. They are also responsible for a first deviation of the load-displacement curve from the initial linear part, which occurs at approximatively 1000 N (or 0.7 J). These initial findings in the first two zones enable us to state that matrix cracking leads to fibre-matrix debonding, which then results in the first delaminations. It is precisely these first delaminations that initiate the first stiffness degradation.

Zone III is limited to displacements between 1.8 and 2.4 mm, i.e. between loads of 1250-1350 and 1500-1650 N and energies of 1.2 and 2.2 J. The SF curve shows the highest drop with a decrease of approximately 7 points, due to major damage events that occur just before and around FLD. In this zone, the 4 classes are detected in different proportions. Class A events are always the most numerous (50% of the signals) followed by class B (23%), class C (16%) and class D (10%) events. Fibre-matrix debonding and delaminations developed significantly, leading to fibre failures. These are clustered in class D and are detected by very energetic signals, explaining the SF drops. Due to the very high energy level of some signals, fibre bundle failures occur at this point, which are located in the centre of the face opposite to indentation. Note that the highest signal energy values are revealed in this zone on Fig. 11b (for energies between 1.8 and 2.2 J) leading to significant drops of SF, a reduction in stiffness and a 50 N drop in load (FLD). Since SF is calculated from the individual AE data, it remains sensitive to the individual high energy AE signal.

After the sharp dropping, SF has more stable behaviour in Zone IV as it shows infinitesimal variations. As mentioned above, all 4 classes are detected but the class B ratio increases by 5 points while class D decreases by 5 points. In addition to the previous failure of some individual fibres or bundles, others still under tension are stretched, leading to new and multiple fibre-matrix debonding. Fibre-related failures are numerically more limited, and their energy levels remain high but much lower than in Zone III up to displacements of 9 mm. Despite this, no severe discontinuities are found in SF. Class D events are not numerous compared to the other three classes, the latter contributing to the gradual increase in cumulative AE energy. Saeedifar et al (Saeedifar et al., 2018) explain that when SF has a constant trend, there is a semi-balance state between the damage mechanisms and some stiffening mechanisms such as fibre bridging. This is consistent with a finding from a previous study. Namely, the morphology of the flax fibres, short and bonded together in bundles to manufacture the twill fabric, enables the creation of a larger amount of fibre bridging which results in a high mode-I interlaminar fracture toughness (G_{Ic}) (Saidane et al., 2019). In the present study, it is also necessary to take into account the sinking of the indenter into the material. The contact area becomes larger as displacement increases. This explains the continued increase in load with the development of damage and thus the constant trend of SF. Note that from 9 mm of displacement (energy of almost 15 J), very energetic events such as those in Zone III reappear, explaining a loss of load which continues gradually (seen on Fig. 5d at 20 J and already mentioned in section 3.1.2). They correspond to the initiation of cracks in the imprint of the indented face mentioned in section 3.2.1. Again, fibre bundle failures occur at this point, with the difference that they are now located on the indented face. These failures, which occur along the circumference of a circle, are the beginnings of a perforation hole resulting from the penetration of the indenter in the specimen.

The chronology of damage mechanisms detected with the AE signals recorded during QSI tests needed to be compared with the mechanisms observed in literature during LVI tests. In a recent study, Sy et al (Sy et al., 2018) described damage evolution in cross-ply flax/epoxy laminates subjected to LVI loading. At the beginning of the damage process, bending cracks originated at the back face of the composite, as observed in QSI and LVI specimens. Matrix cracking, fibre pull-out and debonding were identified as the damage mechanisms initiating the cracks, which is consistent with our findings from the analysis of the AE signals recorded during the QSI tests, in Zones I and II. As the impact energy increased, cracks extended further and further through the composite thickness.

Class A events were detected first and until the end of the QSI test, whatever the energy level. In a study of flax/epoxy woven composite loaded with LVI, Bensadoun et al. (Bensadoun et al., 2017) stated that because of the intrinsic brittleness of the thermoset matrix, matrix cracks were more present than delaminations in thermoset composites. The authors claimed that the limited delaminations were potentially due to the high G_{Ic} of the flax composites, related to several additional energy absorption mechanisms such as crack branching, fibre bridging, etc. The same observation was made in QSI tests, as delamination events (class C) recorded mainly in zones III and IV represented one third of those specific to matrix cracking. Sy et al (Sy et al., 2018) also reported that back face damage on cross-ply flax/epoxy laminates was predominantly fibre-controlled (rather than matrix-controlled), resulting in fibre breakage with limited delamination.

Thus, the results of LVI damage studies available in the literature are consistent with our findings for QSI. SEM and tomographic observations through the specimen thickness and for different energy levels will be conducted in our future work on QSI and LVI specimens in order to consolidate this comparison based on both the damage mechanisms found and their onset sequence.

4. Conclusions

Low velocity impact (LVI) and quasi-static indentation (QSI) tests have been performed on flax-epoxy woven laminates to investigate the similarities between both types of mechanical loading. Specimens were tested at four different energy levels (5, 10, 15 and 20 J), with minimal differences in energy values below 3.9% between QSI and LVI. Similarities were found in load-displacement curves, energy absorption capacity and visible damage. Actually, the differences between QSI and LVI remain low, i.e. 2.1% for linear stiffness, from 0.2 to 5.6% for peak load and less than 7% for the proportions of absorbed energy at 5 and 10 J. LVI and QSI visible damage are similar in shape, i.e. a circular imprint on the impacted or indented face and a cross-shaped mark on the opposite face. The evolution of crack length follows the same trend for both tests until approximately 75% of perforation initiation energy, at which point it reaches a plateau and small cracks appear on the impacted or indented face, indicating the threshold of impactor/indenter penetration. The internal damage within QSI specimens were investigated using acoustic emission (AE). The analysis was based on the acoustic events divided into 4 classes, the use of the Sentry Function and the load-displacement data. Quickly after the beginning of a QSI test, matrix cracks begin to appear and will then continue to develop, leading to the first fibre-matrix debonding and then to the first delaminations. As the energy level approaches 1.8 J, the first fibre failures occur on the back face of specimens, opposite to indentation, and then grow leading to a load drop due to fibre bundle failures. Then, all damage mechanisms already mentioned continue to develop while the load keeps increasing in a saw-tooth pattern until approximately 15 J, corresponding to the indenter penetration threshold. From there, load starts decreasing due to further bundle failures, leading rapidly to the initiation of specimen perforation. This evolution of QSI damage compared with LVI results from the literature suggests similar mechanisms and sequences between both tests, which will be further consolidated by microscopic observations.

Considering our results, QSI testing is a suitable complement to LVI for our material. Moreover, QSI elastic data can be used to shed light on the elastic phase of impact events, where data is limited due to the sampling frequency of the sensors and the impactor velocity. Non-destructive testing techniques such as AE can also be implemented during a QSI test to provide additional information on damage development, which is not always feasible during LVI tests. Finally, QSI tests are cheaper to carry out and easier to investigate, understand and model. As a result, the use of QSI-induced damage in complement to LVI-induced damage is recommended in studies of flax-fibre woven laminates.

Acknowledgements

The authors would like to gratefully acknowledge the urban community of “Grand Reims” and the University of Reims Champagne-Ardenne for their financial supports to the BIOIMPACT project in which this work is conducted.

Declaration of competing interest

The authors declare that they have no known competing financial interests or personal relationships that could have appeared to influence the work reported in this paper.

Funding

This research did not receive any specific grant from funding agencies in the public, commercial, or not-for-profit sectors.

References

Agrawal, S., Singh, K.K., Sarkar, P., 2014. Impact damage on fibre-reinforced polymer matrix composite – A review. J. Compos. Mater. 48, 317–332. https://doi.org/10.1177/0021998312472217

Amiri, A., Triplett, Z., Moreira, A., Brezinka, N., Alcock, M., Ulven, C.A., 2017. Standard density measurement method development for flax fiber. Ind. Crops Prod. 96, 196–202. https://doi.org/10.1016/j.indcrop.2016.11.060

Andrew, J.J., Srinivasan, S.M., Arockiarajan, A., Dhakal, H.N., 2019. Parameters influencing the impact response of fiber-reinforced polymer matrix composite materials: A critical review. Compos. Struct. 224, 111007. https://doi.org/10.1016/j.compstruct.2019.111007

Awais, H., Nawab, Y., Anjang, A., Md Akil, H., Zainol Abidin, M.S., 2020. Effect of fabric architecture on the shear and impact properties of natural fibre reinforced composites. Compos. Part B Eng. 195, 108069. https://doi.org/10.1016/j.compositesb.2020.108069

Baley, C., Gomina, M., Breard, J., Bourmaud, A., Davies, P., 2020. Variability of mechanical properties of flax fibres for composite reinforcement. A review. Ind. Crops Prod. 145, 111984. https://doi.org/10.1016/j.indcrop.2019.111984

Bar, M., Alagirusamy, R., Das, A., Ouagne, P., 2020. Low velocity impact response of flax/polypropylene hybrid roving based woven fabric composites: Where does it stand with respect to GRPC? Polym. Test. 89, 106565. https://doi.org/10.1016/j.polymertesting.2020.106565

Bensadoun, F., Depuydt, D., Baets, J., Verpoest, I., van Vuure, A.W., 2017. Low velocity impact properties of flax composites. Compos. Struct. 176, 933–944. https://doi.org/10.1016/j.compstruct.2017.05.005

Correa, J.P., Montalvo-Navarrete, J.M., Hidalgo-Salazar, M.A., 2019. Carbon footprint considerations for biocomposite materials for sustainable products: A review. J. Clean. Prod. 208, 785–794. https://doi.org/10.1016/j.jclepro.2018.10.099

Cuynet, A., 2018. Etude du comportement mécanique à l'impact et en post impact de matériaux composites à fibres végétales. PhD Thesis, Université Grenoble Alpes, Annecy.

Cuynet, A., Scida, D., Roux, É., Toussaint, F., Ayad, R., Lagache, M., 2018. Damage characterisation of flax fibre fabric reinforced epoxy composites during low velocity impacts using high-speed imaging and Stereo Image Correlation. Compos. Struct., Special issue dedicated to Ian Marshall 202, 1186–1194. https://doi.org/10.1016/j.compstruct.2018.05.090

Dhakal, H.N., Arumugam, V., Aswinraj, A., Santulli, C., Zhang, Z.Y., Lopez-Arraiza, A., 2014. Influence of temperature and impact velocity on the impact response of jute/UP composites. Polym. Test. 35, 10–19. https://doi.org/10.1016/j.polymertesting.2014.02.002

Dicker, M.P.M., Duckworth, P.F., Baker, A.B., Francois, G., Hazzard, M.K., Weaver, P.M., 2014. Green composites: A review of material attributes and complementary applications. Compos. Part Appl. Sci. Manuf. 56, 280–289. https://doi.org/10.1016/j.compositesa.2013.10.014

Feraboli, P., 2006. Some Recommendations for Characterization of Composite Panels by Means of Drop Tower Impact Testing. J. Aircr. 43, 1710–1718. https://doi.org/10.2514/1.19251

Goodarz, M., Bahrami, S.H., Sadighi, M., Saber-Samandari, S., 2019. Low-velocity impact performance of nanofiber-interlayered aramid/epoxy nanocomposites. Compos. Part B Eng. 173, 106975. https://doi.org/10.1016/j.compositesb.2019.106975

Haag, K., Padovani, J., Fita, S., Trouvé, J.-P., Pineau, C., Hawkins, S., De Jong, H., Deyholos, M.K., Chabbert, B., Müssig, J., Beaugrand, J., 2017. Influence of flax fibre variety and year-to-year variability on composite properties. Ind. Crops Prod. 98, 1–9. https://doi.org/10.1016/j.indcrop.2016.12.028

Jusoh, M.S.B.M., Ahmad, H.A.B.I., Yahya, M.Y.B., 2017. Indentation and low velocity impact properties of woven E-glass hybridization with basalt, jute and flax toughened epoxy composites, in: 2017 3rd International Conference on Power Generation Systems and Renewable Energy Technologies (PGSRET). Presented at the 2017 3rd International Conference on Power Generation Systems and Renewable Energy Technologies (PGSRET), pp. 164–168. https://doi.org/10.1109/PGSRET.2017.8251821

Le Duigou, A., Barbé, A., Guillou, E., Castro, M., 2019. 3D printing of continuous flax fibre reinforced biocomposites for structural applications. Mater. Des. 180, 107884. https://doi.org/10.1016/j.matdes.2019.107884

Le Gall, M., Davies, P., Martin, N., Baley, C., 2018. Recommended flax fibre density values for composite property predictions. Ind. Crops Prod. 114, 52–58. https://doi.org/10.1016/j.indcrop.2018.01.065

Liang, S., Guillaumat, L., Gning, P.-B., 2015. Impact behaviour of flax/epoxy composite plates. Int. J. Impact Eng. 80, 56–64. https://doi.org/10.1016/j.ijimpeng.2015.01.006

Malingam, S.D., Ng, L.F., Chan, K.H., Subramaniam, K., Selamat, M.Z., Zakaria, K.A., 2018. The static and dynamic mechanical properties of kenaf/glass fibre reinforced hybrid composites. Mater. Res. Express 5, 095304. https://doi.org/10.1088/2053-1591/aad58e

Minak, G., Morelli, P., Zucchelli, A., 2009. Fatigue residual strength of circular laminate graphite–epoxy composite plates damaged by transverse load. Compos. Sci. Technol., Special Issue on the 12th European Conference on Composite Materials (ECCM12), organized by the European Society for Composite Materials (ESCM) 69, 1358–1363. https://doi.org/10.1016/j.compscitech.2008.05.025

Minak, G., Zucchelli, A., 2008. Damage evaluation and residual strength prediction of CFRP laminates by means of acoustic emission techniques, in: Composite Materials Research Progress. Nova Science Publishers, Inc., pp. 165–207.

Miqoi, N., Pomarede, P., Meraghni, F., Declercq, N., Guillaumat, L., Le Coz, G., Delalande, S., 2021. Detection and evaluation of barely visible impact damage in woven glass fabric reinforced polyamide 6.6/6 composite using ultrasonic imaging, X-ray tomography and optical profilometry. Int. J. Damage Mech. 30, 323–348. https://doi.org/10.1177/1056789520957703

Monti, A., El Mahi, A., Jendli, Z., Guillaumat, L., 2016. Mechanical behaviour and damage mechanisms analysis of a flax-fibre reinforced composite by acoustic emission. Compos. Part Appl. Sci. Manuf. 90, 100–110. https://doi.org/10.1016/j.compositesa.2016.07.002

Muneer Ahmed, M., Dhakal, H.N., Zhang, Z.Y., Barouni, A., Zahari, R., 2021. Enhancement of impact toughness and damage behaviour of natural fibre reinforced composites and their hybrids through novel improvement techniques: A critical review. Compos. Struct. 259, 113496. https://doi.org/10.1016/j.compstruct.2020.113496

Nettles, A.T., Douglas, M.J., 2002. A Comparison of Quasi-Static Indentation Testing to Low Velocity Impact Testing. Compos. Mater. Test. Des. Accept. Criteria. https://doi.org/10.1520/STP10634S

Nisini, E., Santulli, C., Liverani, A., 2017. Mechanical and impact characterization of hybrid composite laminates with carbon, basalt and flax fibres. Compos. Part B Eng. 127, 92–99. https://doi.org/10.1016/j.compositesb.2016.06.071

Pottier, T., Vacher, P., Toussaint, F., Louche, H., Coudert, T., 2012. Out-of-plane Testing Procedure for Inverse Identification Purpose: Application in Sheet Metal Plasticity. Exp. Mech. 52, 951–963. https://doi.org/10.1007/s11340-011-9555-3

Ravandi, M., Teo, W.S., Tran, L.Q.N., Yong, M.S., Tay, T.E., 2017. Low velocity impact performance of stitched flax/epoxy composite laminates. Compos. Part B Eng. 117, 89–100. https://doi.org/10.1016/j.compositesb.2017.02.003

Saeedifar, M., Najafabadi, M.A., Zarouchas, D., Toudeshky, H.H., Jalalvand, M., 2018. Barely visible impact damage assessment in laminated composites using acoustic emission. Compos. Part B Eng. 152, 180–192. https://doi.org/10.1016/j.compositesb.2018.07.016

Saidane, E.H., Scida, D., Pac, M.-J., Ayad, R., 2019. Mode-I interlaminar fracture toughness of flax, glass and hybrid flax-glass fibre woven composites: Failure mechanism evaluation using acoustic emission analysis. Polym. Test. 75, 246–253. https://doi.org/10.1016/j.polymertesting.2019.02.022

Scarponi, C., Sarasini, F., Tirillò, J., Lampani, L., Valente, T., Gaudenzi, P., 2016. Low-velocity impact behaviour of hemp fibre reinforced bio-based epoxy laminates. Compos. Part B Eng. 91, 162–168. https://doi.org/10.1016/j.compositesb.2016.01.048

Scida, D., Assarar, M., Poilâne, C., Ayad, R., 2013. Influence of hygrothermal ageing on the damage mechanisms of flax-fibre reinforced epoxy composite. Compos. Part B Eng. 48, 51–58. https://doi.org/10.1016/j.compositesb.2012.12.010

Serna Moreno, M.C., Horta Muñoz, S., 2020. Mechanical response of ±45° angle-ply CFRP plates under low-velocity impact and quasi-static indentation: Influence of the multidirectional strain state. Compos. Sci. Technol. 194, 108145. https://doi.org/10.1016/j.compscitech.2020.108145

Spronk, S.W.F., Kersemans, M., De Baerdemaeker, J.C.A., Gilabert, F.A., Sevenois, R.D.B., Garoz, D., Kassapoglou, C., Van Paepegem, W., 2018. Comparing damage from low-velocity impact and quasi-static indentation in automotive carbon/epoxy and glass/polyamide-6 laminates. Polym. Test. 65, 231–241. https://doi.org/10.1016/j.polymertesting.2017.11.023

Suresh Kumar, C., Arumugam, V., Santulli, C., 2017. Characterization of indentation damage resistance of hybrid composite laminates using acoustic emission monitoring. Compos. Part B Eng. 111, 165–178. https://doi.org/10.1016/j.compositesb.2016.12.012

Sutherland, L.S., 2018. A review of impact testing on marine composite materials: Part I – Marine impacts on marine composites. Compos. Struct. 188, 197–208. https://doi.org/10.1016/j.compstruct.2017.12.073

Sy, B.L., Fawaz, Z., Bougherara, H., 2018. Damage evolution in unidirectional and cross-ply flax/epoxy laminates subjected to low velocity impact loading. Compos. Part Appl. Sci. Manuf. 112, 452–467. https://doi.org/10.1016/j.compositesa.2018.06.032

Wu, Z., Wu, C., Liu, Y., Cheng, X., Hu, X., 2020. Experimental study on the low-velocity impact response of braided composite panel: Effect of stacking sequence. Compos. Struct. 252, 112691. https://doi.org/10.1016/j.compstruct.2020.112691

Zhang, J., Zhao, L., Li, M., Chen, Y., 2015. Compressive fatigue behavior of low velocity impacted and quasi-static indented CFRP laminates. Compos. Struct. 133, 1009–1015. https://doi.org/10.1016/j.compstruct.2015.08.046

Zuccarello, B., Marannano, G., Mancino, A., 2018. Optimal manufacturing and mechanical characterization of high performance biocomposites reinforced by sisal fibers. Compos. Struct. 194, 575–583. https://doi.org/10.1016/j.compstruct.2018.04.007

Zulkafli, N., Malingam, S.D., Fadzullah, S.H.S.M., Razali, N., 2020. Quasi and dynamic impact performance of hybrid cross-ply banana/glass fibre reinforced polypropylene composites. Mater. Res. Express 6, 125344. https://doi.org/10.1088/2053-1591/ab5f8c

Figure captions

Figure 1. Schematic of the vacuum infusion process

Figure 2. Experimental testing devices: (a) drop tower used for LVI; (b) detailed view of the top of the QSI unit mounted on the Instron testing machine

Figure 3. Typical load-displacement curve (a) and a load-time curve showing the 3 stages (b) of an LVI or QSI test

Figure 4. Superimposed 5, 10, 15 and 20 J load-displacement curves for LVI (a) and QSI (b). The most representative curves have been selected

Figure 5. Superimposed LVI and QSI curves at 5 J (a), 10 J (b), 15 J (c) and 20 J (d). The most representative curves have been selected

Figure 6. Average and standard deviation values of Peak Load for LVI and QSI at each energy level

Figure 7. Absorbed Energy E_a as a function of Total Energy E_t for LVI and QSI

Figure 8. Visible damage on QSI specimens on the indented face (first row) and opposite face (second row) at 5 J (a), 10 J (b), 15 J (c) and 20 J (d)

Figure 9. Visible damage on LVI specimens on the impacted face (first row) and opposite face (second row) of 8-ply samples at 5 J (a), 15 J (b), 25 J (c), 34 J (d) (Cuynet et al., 2018). Note that the speckle pattern on the opposite face was applied for digital image correlation.

Figure 10. Evolution of the average crack length for QSI and LVI (Cuynet et al., 2018) as a function of normalised total energy.

Figure 11. Load-displacement curve superimposed with AE curves showing the number of hits (a), the absolute energy (b) and the Sentry function (c) as a function of impactor displacement at 5 J (first row), 10 J (second row) and 15 J (third row).

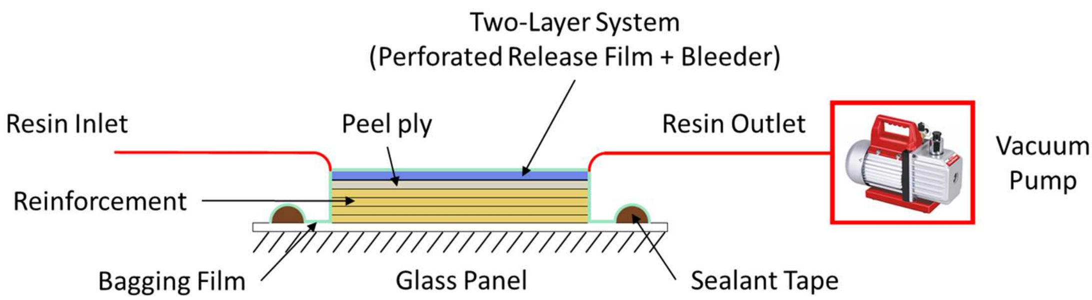
Two-Layer System
(Perforated Release Film + Bleeder)
Resin Inlet
Peel ply
Resin Outlet
Vacuum
Pump
Reinforcement
Bagging Film
Glass Panel
Sealant Tape

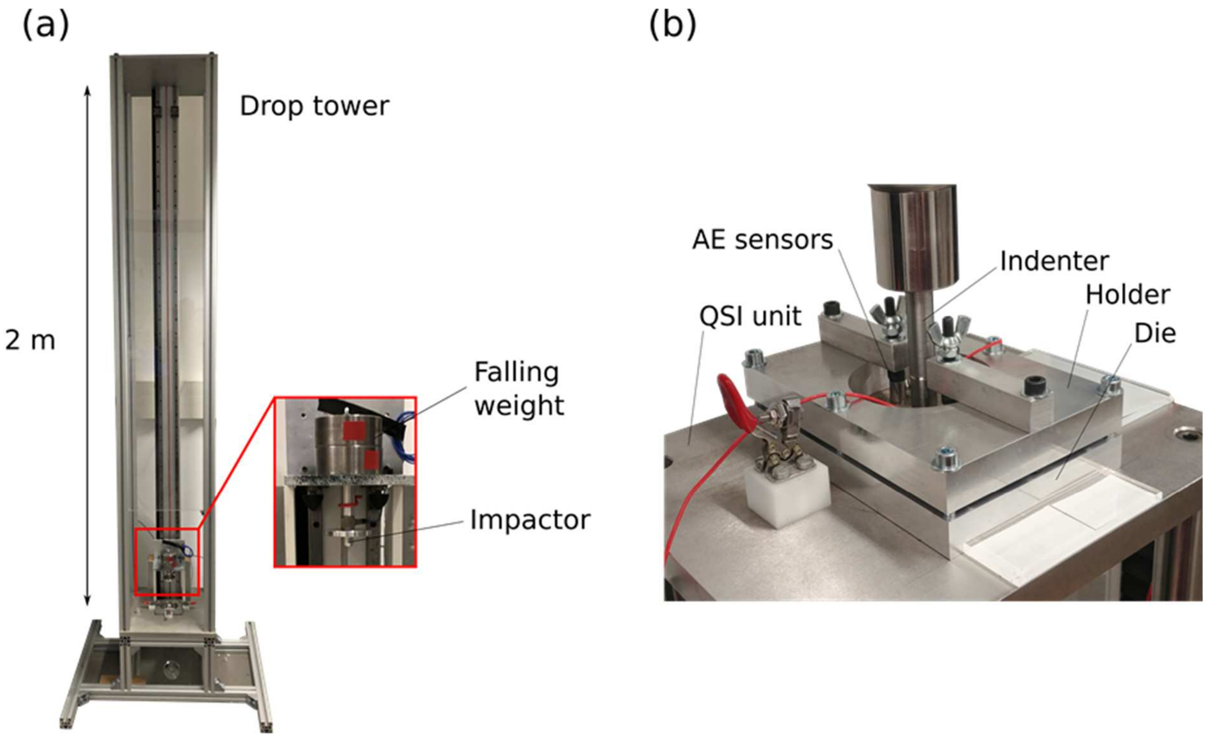
(a)
Drop tower
2 m
Falling
weight
Impactor
(b)
AE sensors
Indenter
Holder
QSI unit
Die

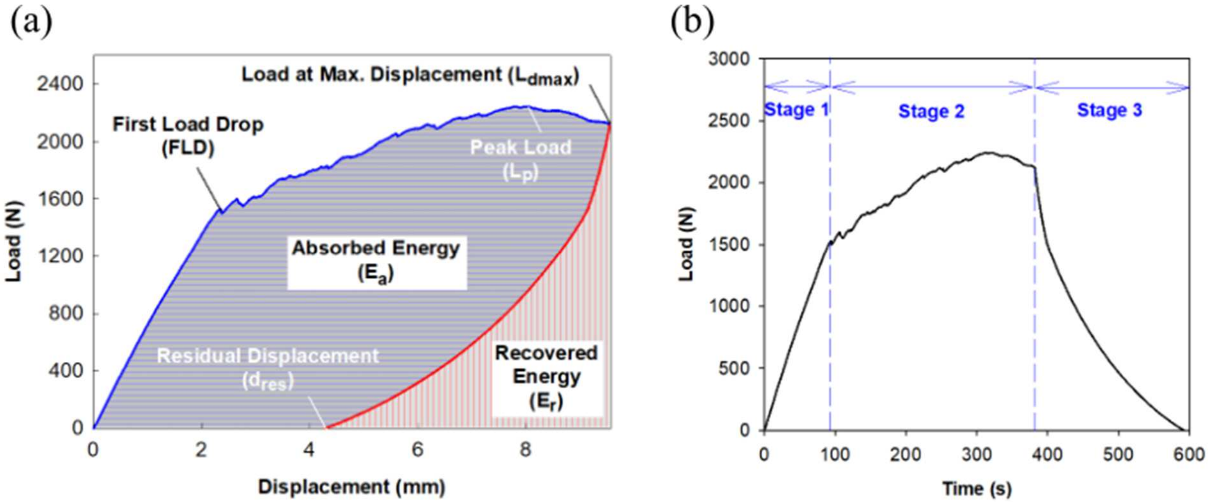

(a)
Load at Max. Displacement (Ldmax)
First Load Drop
(FLD)
Peak Load
(Lp)
Absorbed Energy
(Ea)
Residual Displacement
(dres)
Recovered
Energy
(Er)
Load (N)
Displacement (mm)
(b)
Stage 1
Stage 2
Stage 3
Load (N)
Time (s)

(a) (b)

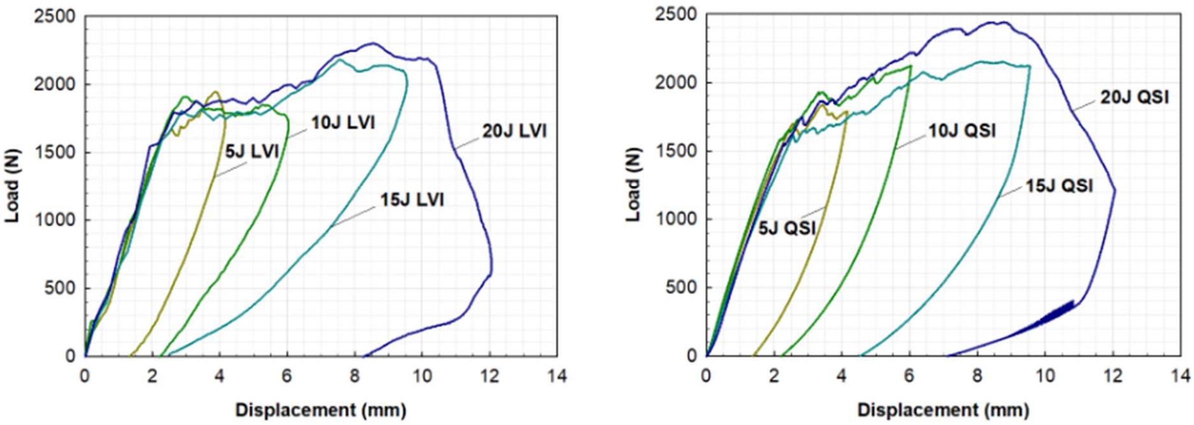
Load (N)
Displacement (mm)
5J LVI
10J LVI
15J LVI
20J LVI
5J QSI
10J QSI
15J QSI
20J QSI

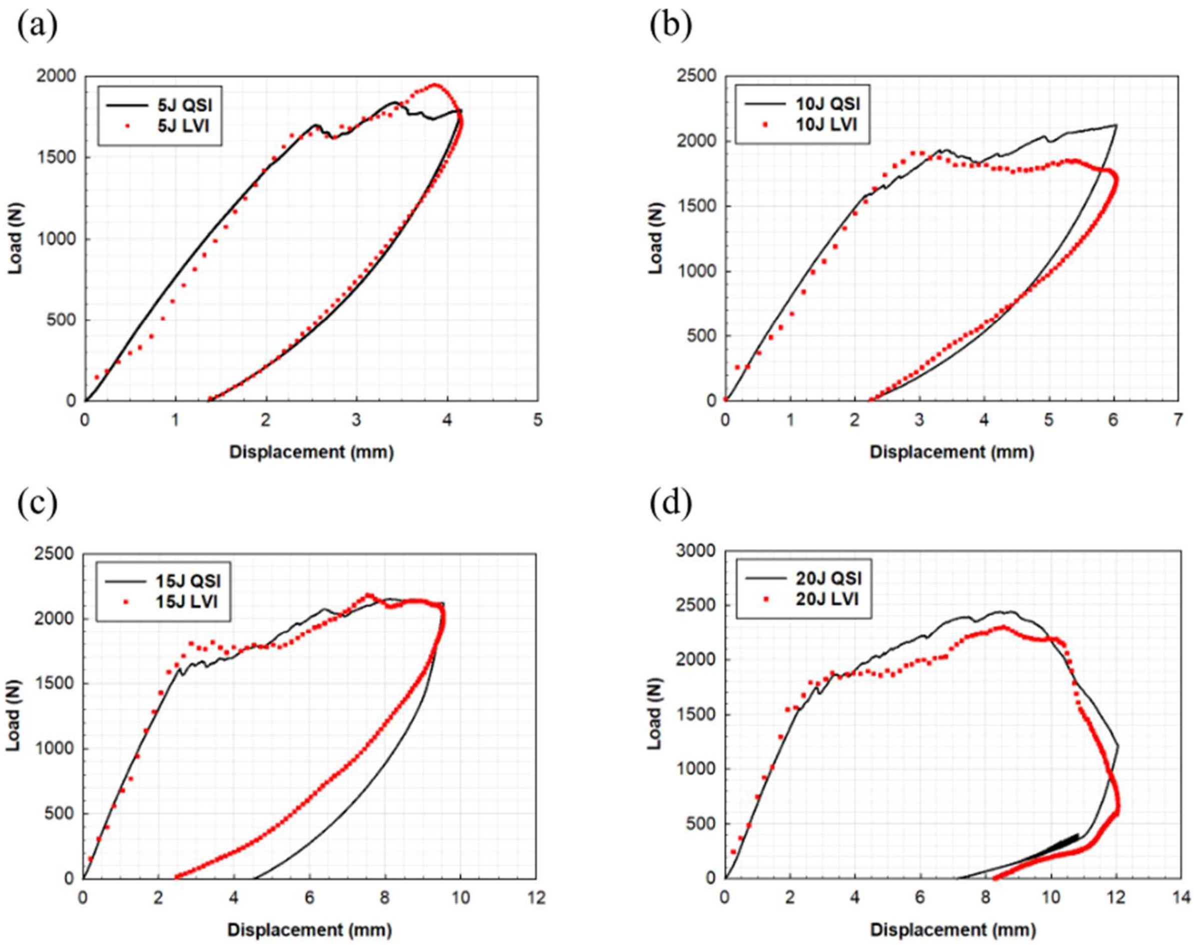
(a)
5J QSI
5J LVI
Load (N)
Displacement (mm)
(b)
10J QSI
10J LVI
Load (N)
Displacement (mm)
(c)
15J QSI
15J LVI
Load (N)
Displacement (mm)
(d)
20J QSI
20J LVI
Load (N)
Displacement (mm)

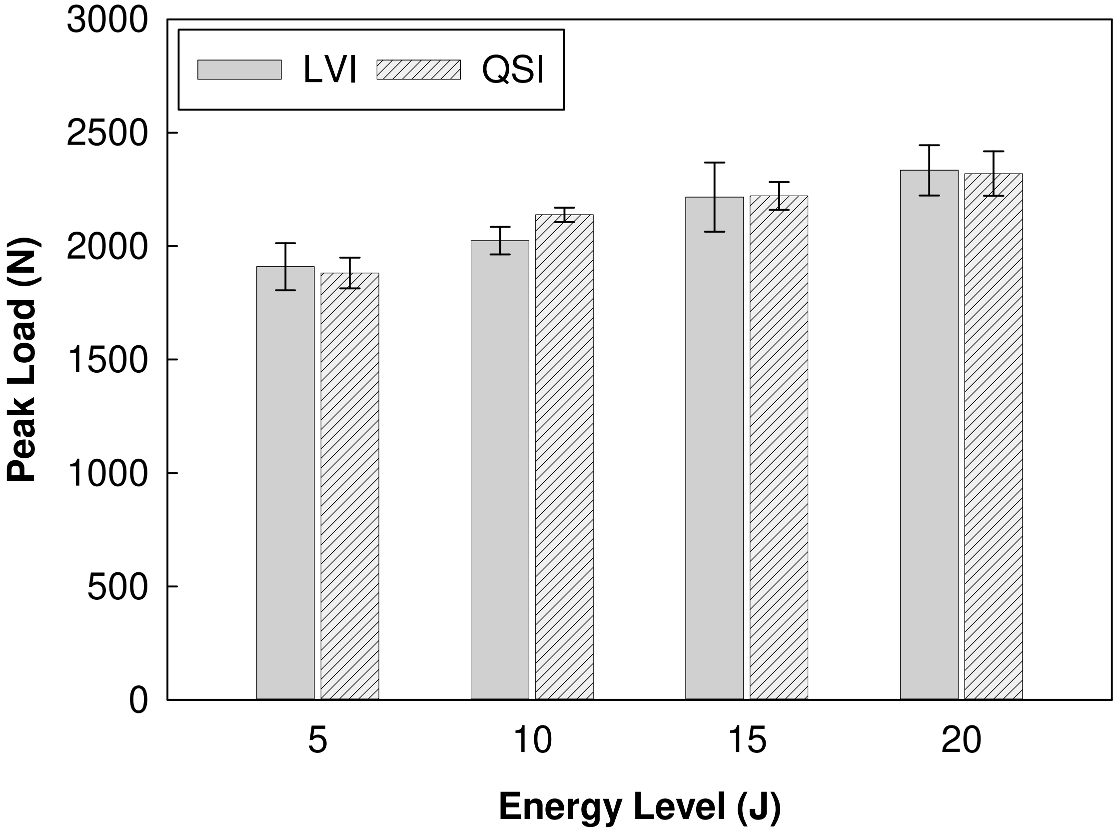

LVI
QSI
Peak Load (N)
0
500
1000
1500
2000
2500
3000
5
10
15
20
Energy Level (J)

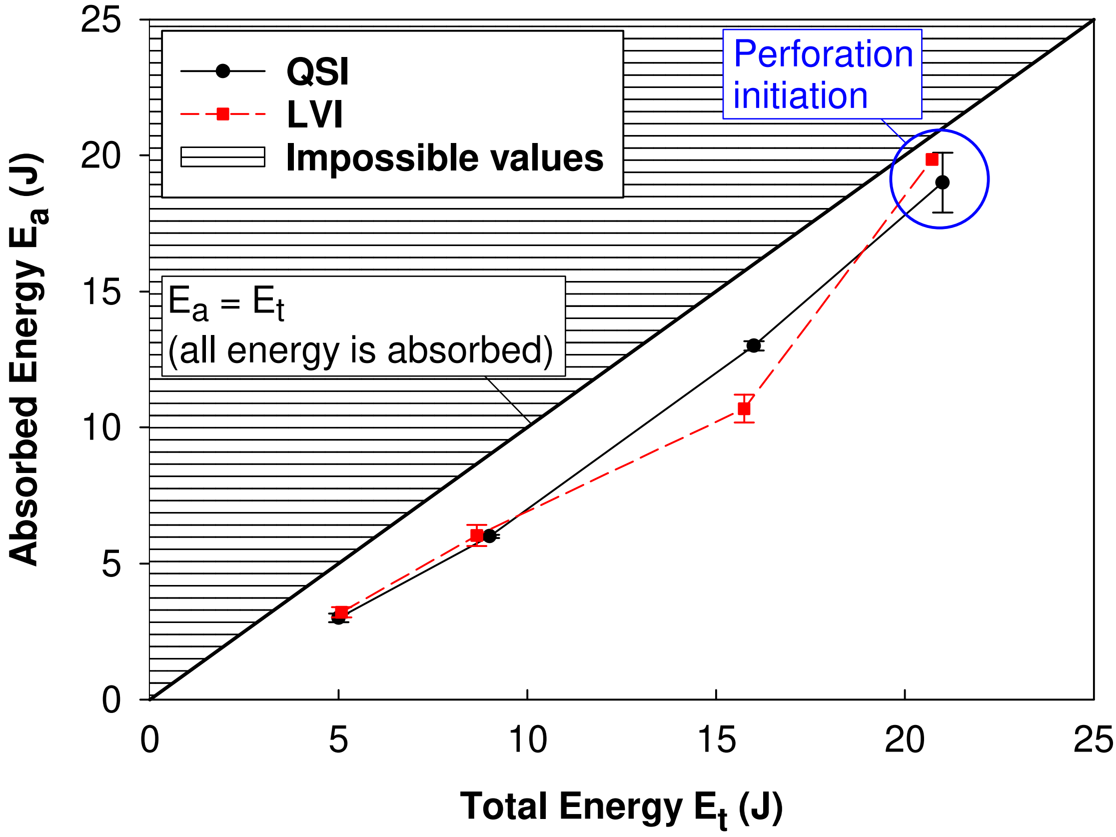
QSI
LVI
Impossible values
Perforation initiation
$E_a = E_t$
(all energy is absorbed)
Absorbed Energy E_a (J)
Total Energy E_t (J)
0
5
10
15
20
25

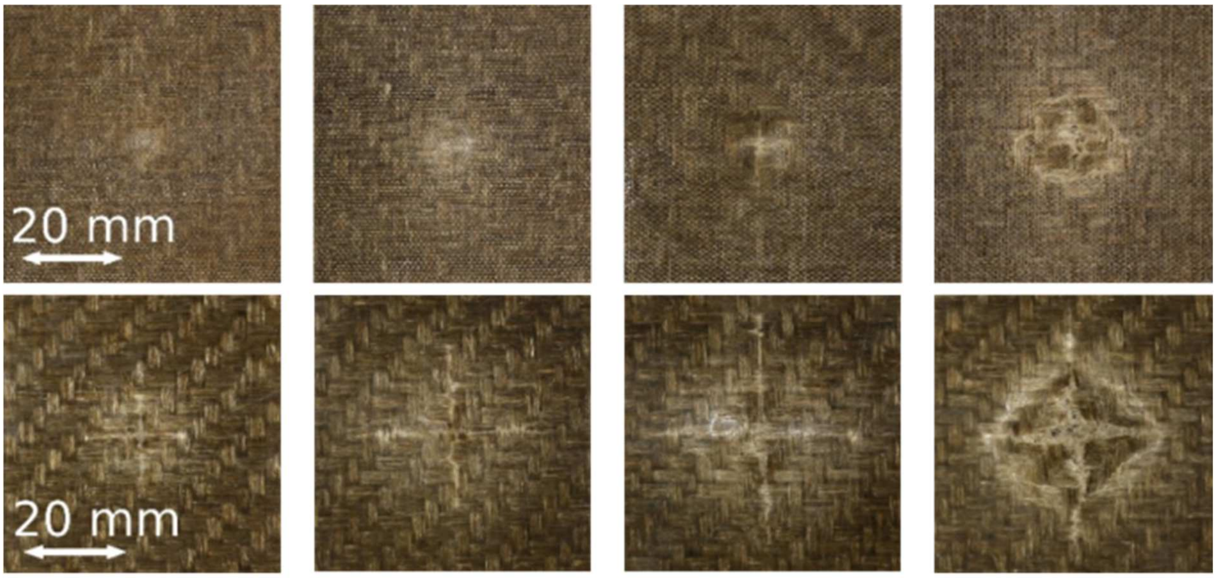

(a) (b) (c) (d)

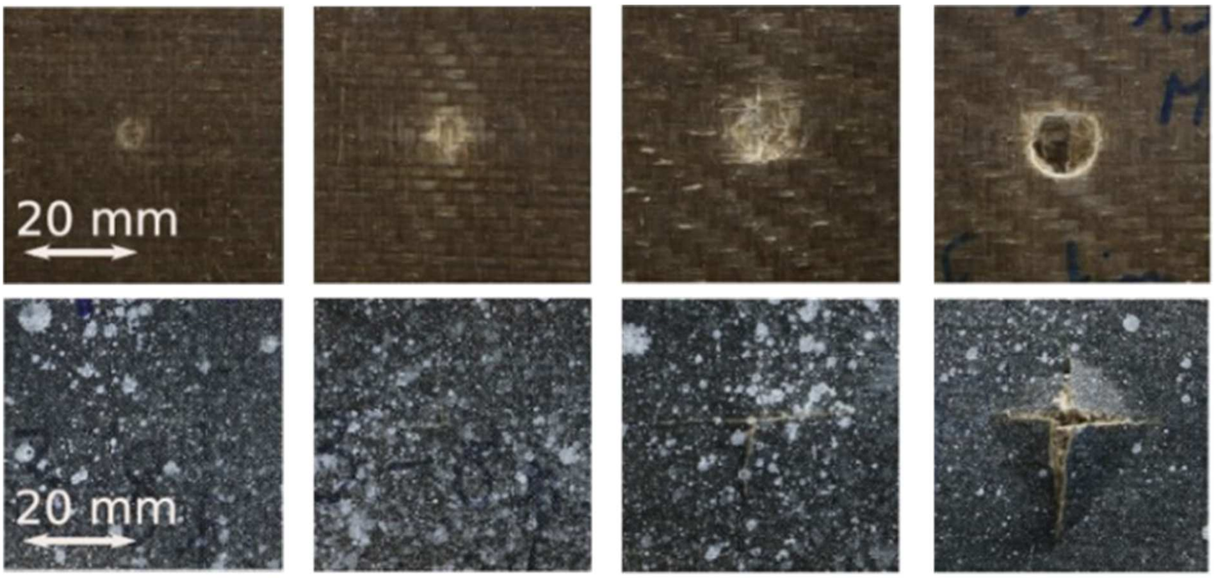

(a) (b) (c) (d)

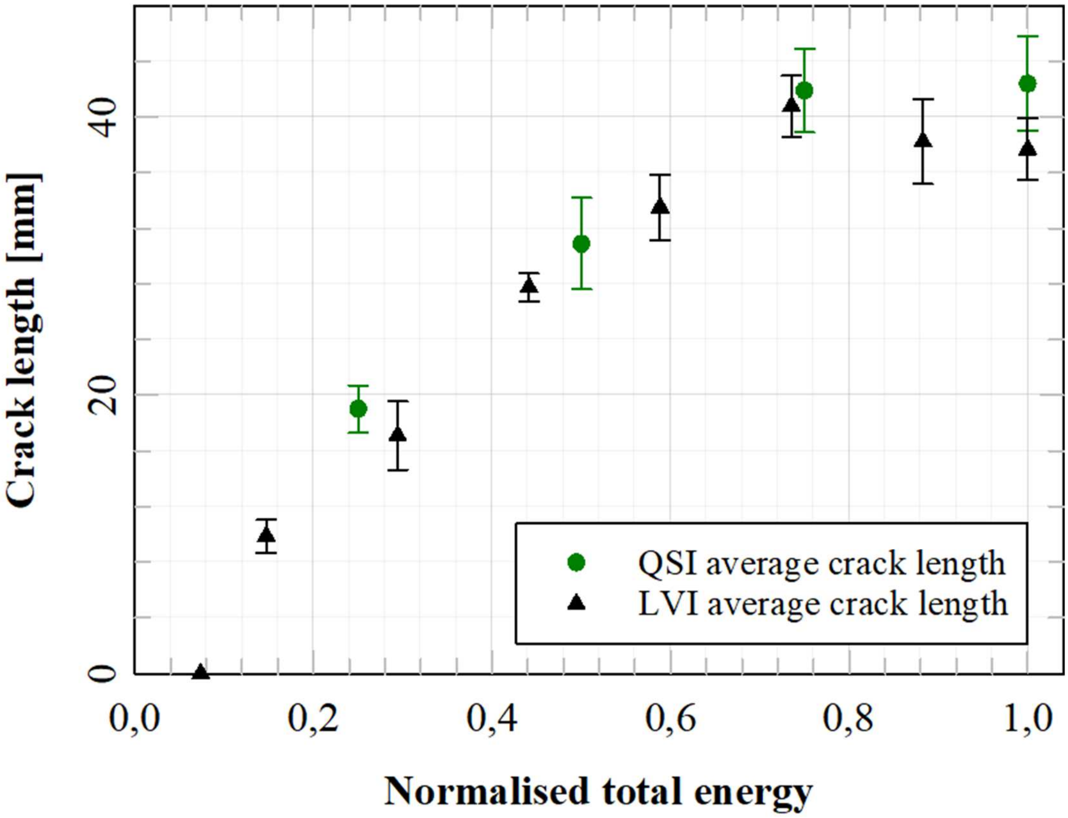

Crack length [mm]
0
20
40
0,0
0,2
0,4
0,6
0,8
1,0
Normalised total energy
QSI average crack length
LVI average crack length

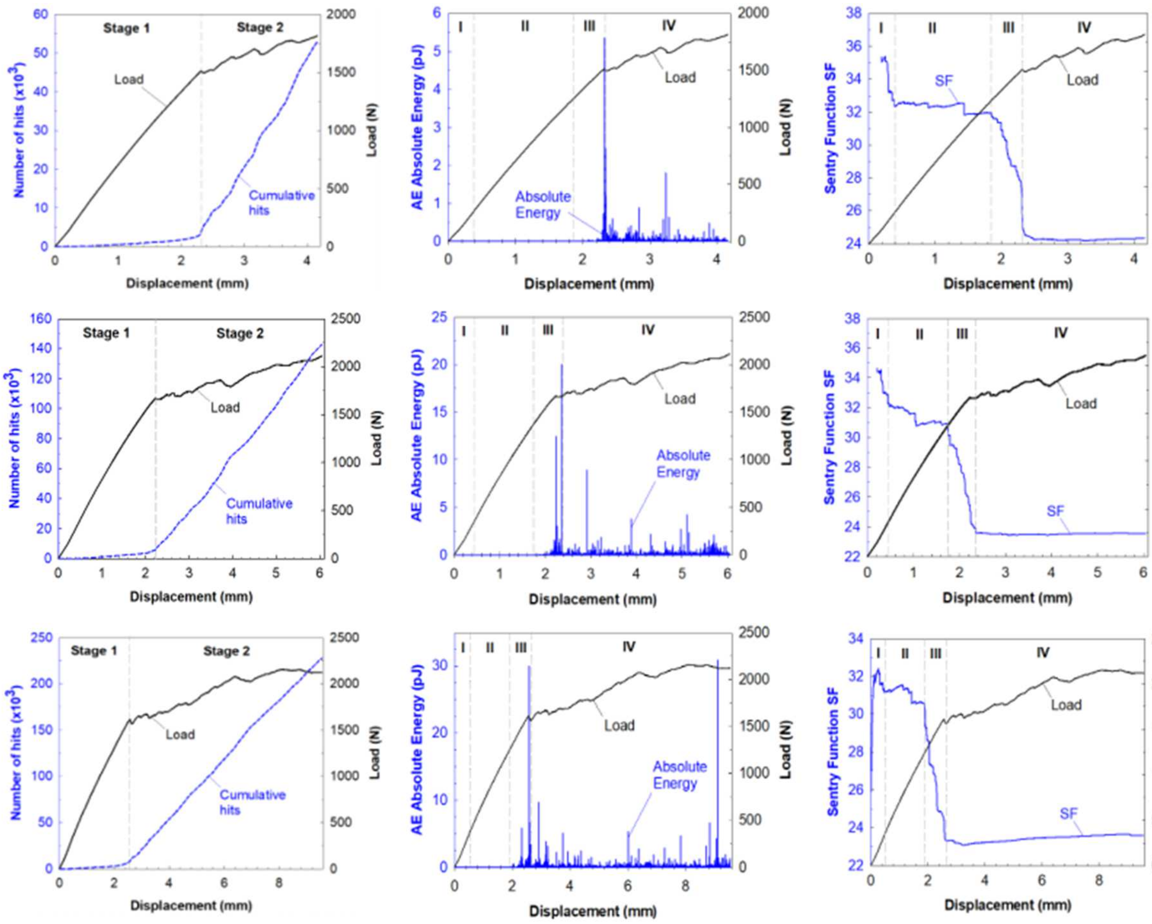
Stage 1
Stage 2
Load
Cumulative hits
Number of hits (x10^3)
Load (N)
Displacement (mm)
I
II
III
IV
Load
Absolute Energy
AE Absolute Energy (pJ)
Load (N)
Displacement (mm)
I
II
III
IV
SF
Load
Sentry Function SF
Load (N)
Displacement (mm)

(a) (b) (c)

Tables

Table 1. Main characteristics of Stage 1, the relatively linear part of load-displacement curves.

	LVI	**QSI**
Linear Stiffness	710 ± *55* N/mm	695 ± *51* N/mm
Load at FLD	1785 ± *111* N	1548 ± *62* N
Displacement at FLD	2.66 ± *0.28* mm	2.32 ± *0.17* mm

Table 2. Total (E_t) and absorbed (E_a) energies and E_a / E_t ratio for LVI and QSI at all four energy levels.

		Total Energy E_t **(J)**	**Absorbed Energy** E_a **(J)**	E_a / E_t **(%)**
5 J	**LVI**	4.92 ± *0.22*	3.08 ± *0.19*	62.6
	QSI	5.11 ± *0.18*	3.21 ± *0.16*	62.8
10 J	**LVI**	8.97 ± *1.16*	5.80 ± *0.39*	64.7
	QSI	9.17 ± *0.05*	6.36 ± *0.05*	69.4
15 J	**LVI**	15.76 ± *0.73*	10.71 ± *0.51*	68.0
	QSI	15.99 ± *0.24*	12.55 ± *0.16*	78.5
20 J	**LVI**	20.79	19.92	95.8
	QSI	21.15 ± *0.92*	19.15 ± *1.10*	90.5